European Journal of Radiology 156 (2022) 110555

Contents lists available at ScienceDirect

European Journal of Radiology

journal homepage: www.elsevier.com/locate/ejrad

A patient-informed approach to predict iodinated-contrast media enhancement in the liver

Hananiel Setiawan [a,b,e,*], Chaofan Chen [c], Ehsan Abadi [a,b,e,f,h], Wanyi Fu [a,b,f], Daniele Marin [e,h], Francesco Ria [a,b,d], Ehsan Samei [a,b,d,e,f,g,h,i]

[a] Carl E. Ravin Advanced Imaging Laboratories, Department of Radiology, Duke University, 2424 Erwin Rd, Ste. 302, Durham, NC 27705, USA
[b] Center for Virtual Imaging Trials, Duke University, 2424 Erwin Rd, Ste. 302, Durham, NC 27705, USA
[c] School of Computing and Information Science, The University of Maine, 5711 Boardman Hall, Room 348, Orono, ME 04469, USA
[d] Clinical Imaging Physics Group, Duke University Health System, 2424 Erwin Rd, Ste. 302, Durham, NC 27705, USA
[e] Graduate Program in Medical Physics, School of Medicine, Duke University, 2424 Erwin Rd, Ste. 302, Durham, NC 27705, USA
[f] Department of Electrical and Computer Engineering, Pratt School of Engineering, Duke University, 305 Nello L. Teer Engineering Building, Box 90271, Durham, NC 27708, USA
[g] Department of Biomedical Engineering, Pratt School of Engineering, Duke University, 305 Nello L. Teer Engineering Building, Box 90271, Durham, NC 27708, USA
[h] Department of Radiology, School of Medicine, Duke University, Box 3808 DUMC, Durham, NC 27710, USA
[i] Physics Building, Science Drive Campus, Box 90305, Durham, NC 27708, USA

ARTICLE INFO

Keywords:
contrast-enhanced CT
contrast CT
Iodinated contrast enhancement
Contrast perfusion
Liver enhancement

ABSTRACT

Objective: To devise a patient-informed time series model that predicts liver contrast enhancement, by integrating clinical data and pharmacokinetics models, and to assess its feasibility to improve enhancement consistency in contrast-enhanced liver CT scans.

Methods: The study included 1577 Chest/Abdomen/Pelvis CT scans, with 70–30% training/validation-testing split. A Gaussian function was used to approximate the early arterial, late arterial, and the portal venous phases of the contrast perfusion curve of each patient using their respective bolus tracking and diagnostic scan data. Machine learning models were built to predict the Gaussian parameters of each patient using the patient attributes (weight, height, age, sex, BMI). Pearson's coefficient, mean absolute error, and root mean squared error were used to assess the prediction accuracy.

Results: The integration of the pharmacokinetics model with a two-layered neural network achieved the highest prediction accuracy on the test data ($R^2 = 0.61$), significantly exceeding the performance of the pharmacokinetics model alone ($R^2 = 0.11$). Applying the model demonstrated that adjusting the contrast administration directed by the model may reduce clinical enhancement inconsistency by up to 40 %.

Conclusions: A new model using a Gaussian function and supervised machine learning can be used to build liver parenchyma contrast enhancement prediction model. The model can have utility in clinical settings to optimize and improve consistency in contrast-enhanced liver imaging.

1. Introduction

The majority of clinical CT imaging in the United States involves iodinated-contrast materials [1]. The enhanced tissue contrast can thus improve the depiction of a variety of disorders for diagnostic purposes in target organs, including liver, kidneys, spleen, pancreas, brain, and lungs. Many studies have indicated the correlation between contrast enhancement and patient weight or other body habitus metrics [2–11], the variability of which, across patients, leads to variability in tissue enhancement. However, despite this variability, there has been limited effort to standardize or optimize contrast administration techniques. One common approach in many institutions is to use the same dose and

Peer review under responsibility of If file "editor conflict of interest statement" is present in S0, please extract the information and add it as a footnote (star) to the relevant author. The sentence should read (and be amended accordingly): Given his/her role as EditorinChief/Associate Editor/Section Editor <NAME of Editor> had no involvement in the peerreview of this article and has no access to information regarding its peerreview.

* Corresponding author at: Tel.: +19196841410. 2424 Erwin Rd, Ste. 302, Durham, NC 27705, USA.
E-mail address: hananiel.setiawan@duke.edu (H. Setiawan).

https://doi.org/10.1016/j.ejrad.2022.110555
Received 6 March 2022; Received in revised form 20 July 2022; Accepted 7 October 2022
Available online 13 October 2022

Table A1
Demographic of the clinical data in the training set. **A.2.** Demographic of the clinical data in the testing set **A.3.** Summary of examinations included in the study by clinical protocols, scanners, and scan parameters; Noise Index (NI) for GE Healthcare scanners; Quality Reference Effective mAs (Q) for Siemens Healthineers scanners.

Training				
Table A.1	Mean	Median	Range [min, max]	Std. Dev.
Height (cm)	170.5	170.2	[139.7, 198.1]	10.5
Weight (kg)	81.9	80.1	[40.8, 138.3]	19.0
BMI (kg/m^2)	28.2	27.3	[14.0, 53.7]	6.4
Age (y)	55.2	57.0	[13.0, 97.0]	17.4
Contrast Bolus Volume (mL)	145.1	145.0	[141.0, 149.0]	1.7
Average Injection Rate (mL/s)	2.9	2.9	[2.8, 3.0]	0.02
Start-of-Injection to Scan Duration interval (s)	65.3	65.0	[54.0, 98.0]	7.4
Testing				
Table A.2	Mean	Median	Range [min, max]	Std. Dev.
Height (cm)	171.0	171.0	[147.3, 195.6]	9.9
Weight (kg)	82.4	80.9	[38.9, 135.7]	18.7
BMI (kg/m^2)	28.3	26.9	[11.0, 53.7]	6.7
Age (y)	56.3	59.0	[12.0, 99.0]	16.7
Contrast Bolus Volume (mL)	145.0	145.0	[136.0, 154.0]	2.5
Average Injection Rate (mL/s)	2.9	2.9	[2.9, 3.0]	0.02
Start-of-Injection to Scan Duration interval (s)	65.5	65.0	[46.0, 98.0]	7.8

Table A.3

Vendor	Models	Slice Thickness	Noise Index (GE), Quality Reference mAs (Siemens)	kV	Pitch
Siemens Healthineers	SOMATOM Definition Flash, Force	0.6 mm	150, 200	120	0.8
GE Healthcare	Discovery CT750HD, Revolution, VCT	0.625 mm	19.2, 22.0	120	1.38

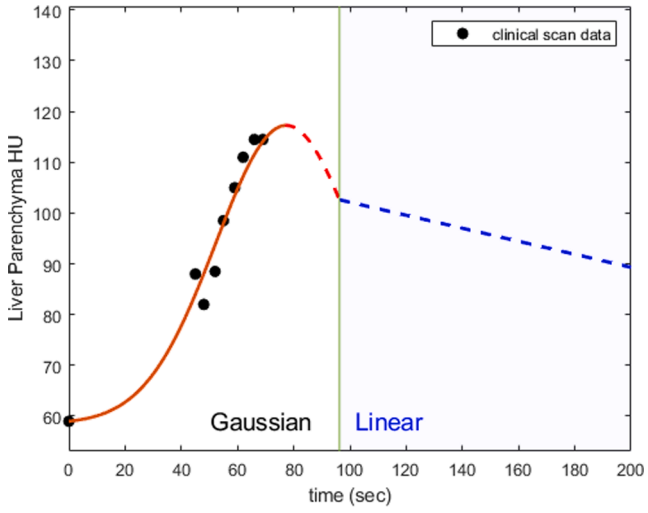

Fig. A1. Illustration of the Gaussian fitting using patient clinical data. The base HU was re-added after the Gaussian fitting process for illustration purposes.

Table B1
Optimization constraints for the Gaussian parameters fitting.

Variable	Minimum	Maximum
σ	20 s	30 s
A	0.95*(Observed Maximum Value for the Given Patient) HU	1.05*(Observed Maximum for the Given Patient) HU
μ	0.85*(Time when Observed Maximum is Achieved for the Given Patient) second	1.15*(Time when Observed Maximum is Achieved for the Given Patient) second

injection flow rate for every patient, while others make minor adjustment based on patient weight thresholds [12,13]. The majority of the contrast-enhanced CT scans in our institution use 300 mgI/mL contrast media; in limited circumstances or protocols, different iodine concentration of the contrast media (e.g. 370 mgI/mL) is also occasionally used. Inconsistencies of these approaches and of these customization lead to inconsistences in contrast enhancement across patients, exacerbating clinical diagnostic risk, especially in under- and over-enhanced patient scans [14].

Table C1
Brief descriptions of each algorithms used.

Algorithm	Description
SVM	Linear kernel
Gaussian Process	Squared exponential kernel, constant basis
Linear Regression	Least-square regression, stochastic gradient descent
Trees	MSE splits, 1 min leaf size, 10 min parent size
Ensemble Trees	Least-square boosting
Neural Network	2 hidden layers of 10 and 4 nodes
GAM	300 trees/predictor, 100 trees/interaction
Gaussian Kernel Regression	LBFGS solver, L2 regularization

To improve consistency in contrast enhanced CT exams, several models have been proposed to prospectively characterize contrast enhancement dynamics (i.e., how contrast media perfuses) in a particular organ of interest using known patient attributes. Existing models rely primarily on mathematical pharmacokinetics approximation, not necessarily individualized to patient attributes. One such model is the Physiology-based Pharmacokinetics (PBPK) model [15,16]. The PBPK model is a differential-equation based, compartmental model which predicts contrast enhancement dynamics after injection across different organs as a function of time for an average population. While the PBPK model has been demonstrated to agree with averages across patient cases [16], it may not sufficiently provide individualization to patient-specific attributes [17,18]. To reduce the clinical consistencies and to ensure proper contrast enhancement, there is a need to build a contrast perfusion model which considers patient-specific attributes.

This study aimed to build a contrast enhancement model that supplements the PBPK model and patient data. In doing so, the goal was to take advantage of the knowledge embedded in the PBPK model but supplement it with additional insights that can be gained through neural network analysis of clinical data. The utility of such an integrated approach was further tested in a hypothetical study by investigating how much consistency in contrast enhancement in the liver can be improved if the model were to be applied to inform contrast administration protocols.

Table D1
Summary of the goodness-of-fit of the prediction models. **D.2.** Summary of the goodness-of-fit of the prediction models at time of diagnostic scan. The MAE and RMSE are in the Hounsfield Unit (HU).

Table D.1

	SVM	Gaussian Process	Trees	Ensemble Trees	**Neural Net**	GAM	Linear Regr.	Gaussian Kernel	PBPK
Test R^2	0.60	0.60	0.45	0.51	**0.61**	0.58	0.58	0.57	0.11
MAE	10.76	10.78	12.76	11.70	**10.67**	11.01	11.00	11.63	37.84
RMSE	13.50	13.51	26.12	14.87	**13.48**	13.79	13.85	14.52	42.11

Table D.2

	SVM	Gaussian Process	Trees	Ensemble Trees	**Neural Net**	GAM	Linear Regr.	GaussianKernel	PBPK
Test R^2	0.58	0.59	0.46	0.48	**0.60**	0.57	0.55	0.48	0.01
MAE	10.08	10.03	12.76	12.60	**9.89**	10.66	10.56	11.38	18.95
RMSE	13.09	13.04	16.22	16.21	**12.87**	13.51	13.60	14.65	23.97

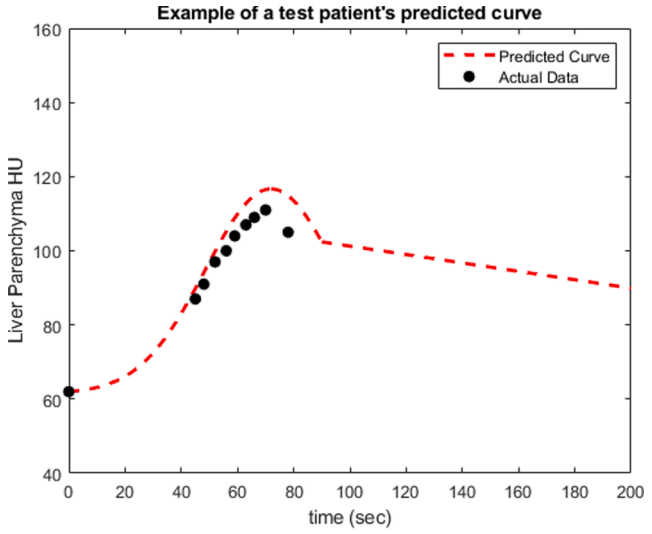

Fig. B1. Example of a test patient's predicted curve (red dotted line) as compared to the ground truth clinical data.

2. Material and methods

2.1. Clinical data

This IRB-approved retrospective study included contrast-enhanced Chest-Abdomen-Pelvis (CAP) CT examinations of 7473 adult patients which were conducted using standard clinical protocols at the Medical Center from 2015 to 2018. From this cohort, 1577 cases (736 female, 841 male) with complete clinical information, such as their height, weight, age, and biological sex, were selected for the study. For each exam, patient attributes (height, weight, age, and biological sex), scanner parameters (CT vendor/type, tube potential, slice thickness, scan times), as well contrast administration protocol (bolus volume, concentration, flow rate, injection duration) were collected using a quality and safety monitoring system (METIS, Duke University, Durham NC), which provides a database of scanner specifics, acquisition parameters, $CTDI_{vol}$, and patient size that is calculated as the patient effective diameter, and a contrast management system (NEXO, Bracco Diagnostics, Monroe Township, NJ). All patients were prescribed with the same contrast media administration protocol of 150 mL of iopamidol with a concentration of 300 mgI/mL at 3 mL/s uniphasic injection flow rate. In actuality, the patients received 145.6 ± 2.5 mL of 300 mgI/mL iopamidol contrast media and an injection rate of 2.9 ± 0.1 mL/s. Only 5 of the 1577 patients were recorded to have received saline flush after iodine injection. In addition, the CT scanning exam included a bolus tracking contrast monitoring series to determine the appropriate scan start time; these images were consecutively acquired every 3 s, starting from 45 s after the injection, to monitor whether the organ of interest (ROI in liver) has received adequate contrast enhancement before commencing the diagnostic scan. 70 % of the patient cases were used for training the model, while 30 % were used for testing the trained model. The summary of the clinical data and acquisition parameters are provided in Table A1**, A2, and A3**.

In addition, we estimated the organ dose-based effective dose for all the patients following the ICRP Publication 103 and using a Monte Carlo patient-specific organ doses estimation, validated in a previous study [1,19].

2.2. Image segmentation

The scan protocol for each patient included 3 types of data: 1) pre-monitoring image, taken unenhanced before contrast injection starts, 2) monitoring images, taken after contrast media was injected during the bolus tracking period, and 3) diagnostic image series. The livers were automatically segmented in the acquired images using a deep learning-based algorithm previously developed by our team [20]. This segmentation tool, previously trained on 200 manually segmented CT images, is able to identify major body organs, including liver, with dice similarity coefficient values > 0.85. The HU value of the segmented livers was used to represent the enhancement value; the median was used to minimize the influence of the HU values of non-parenchyma structures, such as vasculature.

2.3. Model development

According to the PBPK model and other studies, the shape of the liver contrast enhancement dynamic curve for uniphasic, constant contrast injection protocol over time can be represented by a Gaussian rise to a peak followed by a linear decline before the slope gradually stabilizes, shown in Fig. A1 [16,21]. The Gaussian section of the curve represents the early arterial, late arterial, and the portal venous phases, while the gradual decline represents the washout/delayed phase. In this study, we thus used a Gaussian function as shown in.

$$\mathbf{3.}\quad f_{patient}(t) = \frac{A}{1-\exp\left(-\frac{B^2}{2\sigma^2}\right)} * \left(\exp\left(-\frac{(t-B)^2}{2\sigma^2}\right) - \exp\left(-\frac{B^2}{2\sigma^2}\right)\right) \textbf{(Eq. A)}$$

to approximate the early arterial, late arterial, and the portal venous phases of the contrast perfusion curve from a single patient. A is the peak value of the Gaussian function, B is the time at which the peak value occurs, and σ controls how fast the curve rises. Note that the Gaussian function in **Equation A** has value of 0 at time t = 0, i.e., f(0) = 0, so that the function f approximates the *relative* HU values, which are HU values minus the base HU values of a given patient.

As the first step in the modeling process, we applied a least-square fit to each training patient's contrast enhancement data (bolus tracking and diagnostic scans) by a Gaussian curve f(t) on the contrast enhancement values of both the bolus tracking and diagnostic scans, with the base HU values subtracted, to obtain the corresponding Gaussian parameters A,

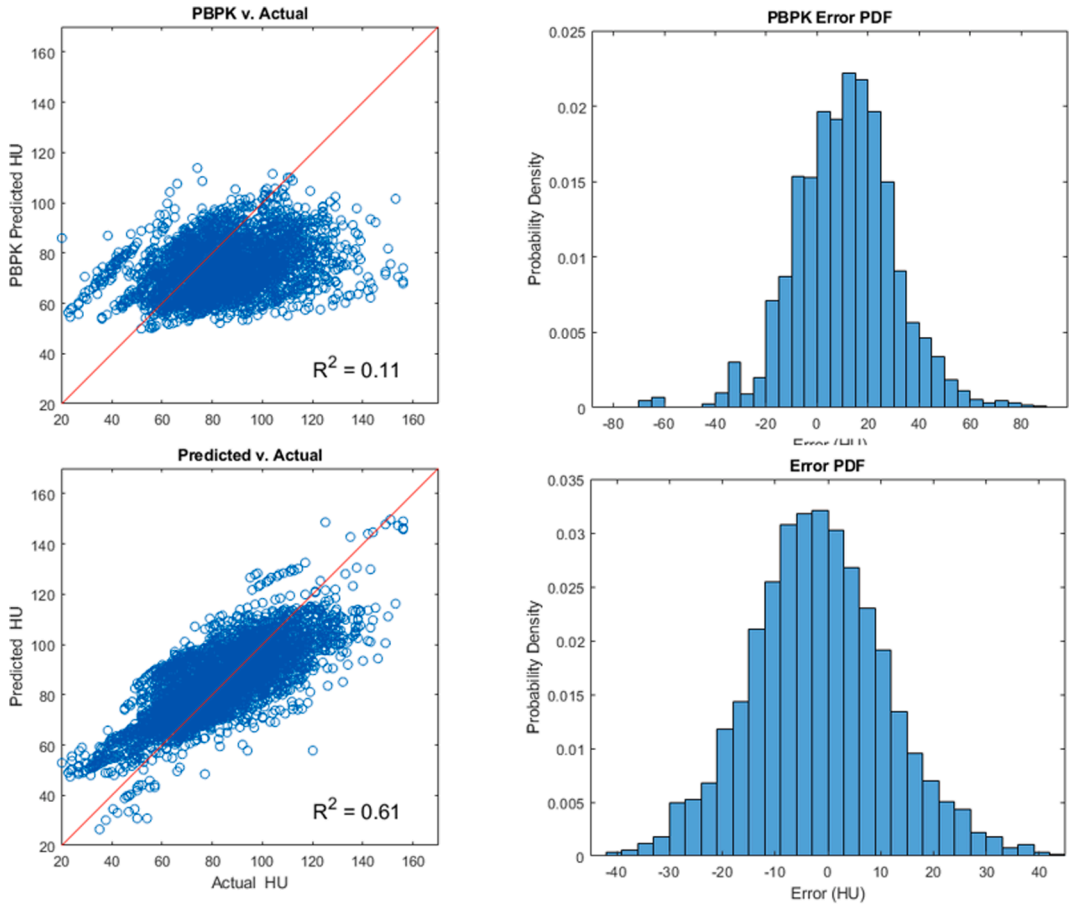

Fig. C1. (Top Left) Prediction of Test Patients using PBPK as compared to actual clinical data. (Top Right) Error Probability Density Function of the PBPK prediction. (Bottom Left) Prediction of Test Patients using the patient-informed, neural network model as compared to actual clinical data. (Bottom Right) Error Probability Density Function of the neural network model prediction.

B, and σ for that patient. The parameters A, B, and σ obtained for all the training patients were then used as the ground-truth regression targets for our machine learning models. The Gaussian parameter values were constrained as shown in Table B1**.** Due to the unavailability of data beyond the diagnostic scan time, we were only able to fit the early arterial, late arterial, and the portal venous phases (i.e., the Gaussian part) of the contrast perfusion curve; the washout/delayed phase was based on the general average slope from the PBPK result of the XCAT phantom library [16] (see Fig. A1).

As the second step in the modeling process, the training (70 %) and testing (30 %) datasets were randomly selected, with female patients making up 47 % of the training set and 45 % of the testing set. We trained several machine learning models to predict the peak value (A), peak time (B), and how fast the curve rises (σ) from patient attributes. In particular, we used multiple regression algorithms to build a prediction model: support vector machine (SVM) regression, Gaussian process regression, linear regression, regression trees, ensemble of regression trees, neural networks, generalized additive model (GAM), and Gaussian kernel regression (Table C1).

All models were validated using a 10-fold cross validation strategy. We trained the models using the training patients' height, weight, BMI, age, sex, pre-injection liver CT number (Base HU) as the predictors, and the Gaussian parameters values of A, B, and σ of the corresponding training patients obtained previously as the ground-truth regression targets. For testing, given a previously unseen test patient, the machine learning models predicted A, B, and σ of the test patient from the patient's attributes. The predicted Gaussian parameters of the test patient were then used to reconstruct the curve f(t) and the liver contrast enhancement dynamic curve of that patient (f(t) + Base HU). We measured the accuracy of the prediction by comparing the predicted curve values with the observed clinical scan values of the liver parenchyma using R^2 value. In addition to R^2, the goodness-of-fit was evaluated using mean absolute error and root mean squared error.

3.1. *Demonstration of clinical implication*

The main potential benefit of implementing a predictive model to adjust contrast administration protocol is to improve consistency of contrast enhancement across patients. To illustrate such a goal, we used the prediction model to retrospectively predict what the HU value of the liver of the test set could have been achieved if the model could have been prospectively applied. We then adjusted the contrast media concentration, assuming a linear relationship between contrast media concentration and organ contrast enhancement [11], such that the parenchyma enhancement in HU is within the median clinically acceptable range of 92 to 132 HU as recommended by [22]. Lastly, we compared the consistency of the parenchyma enhancement level in our patient cases before and after the theoretical application of this predictive model using the Kruskal Wallis test.

4. Results

4.1. *Prediction models*

All the proposed patient-informed models yielded greater predictive accuracy (R^2) and lower mean absolute error (MAE) and root mean squared error (RMSE) than PBPK alone. In particular, the neural network model achieved the highest predictive accuracy, test R^2 of 0.61,

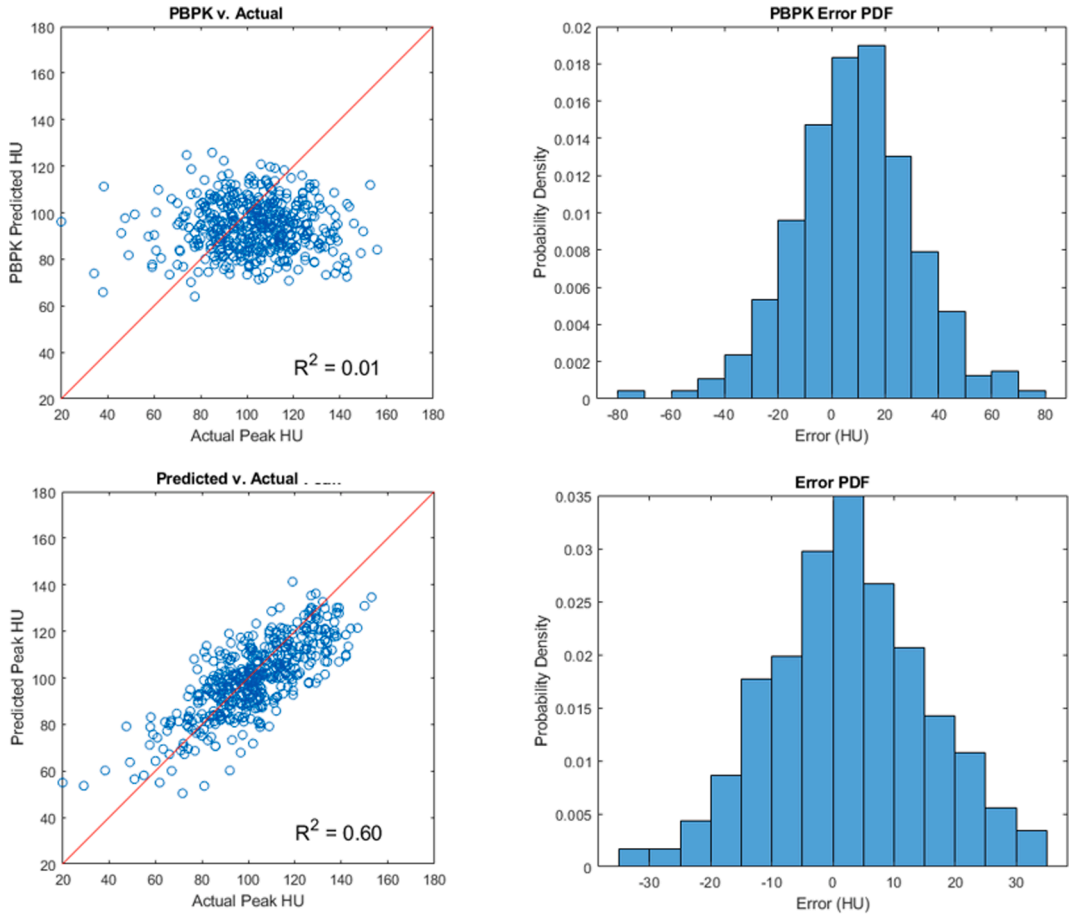

Fig. D1. (Top Left) Prediction of Test Patients using PBPK as compared to actual clinical data at time of diagnostic scan. (Top Right) Error Probability Density Function of the PBPK prediction at time of diagnostic scan. (Bottom Left) Prediction of Test Patients using the patient-informed, neural network model as compared to actual clinical data at time of diagnostic scan. (Bottom Right) Error Probability Density Function of the neural network model prediction at time of diagnostic scan.

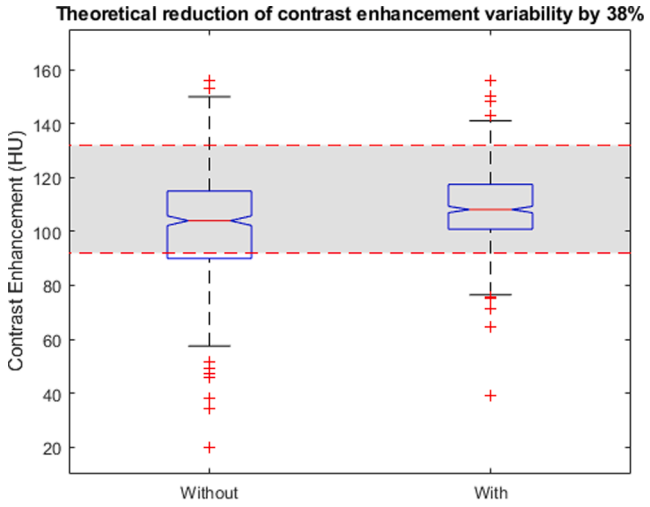

Fig. E1. Box plots demonstrating the effect of applying the prediction model to adjust the concentration of contrast media (p-value < 0.001).

and lowest MAE and RMSE, 10.67 HU and 13.48 HU, respectively, compared to other models we used when compared to the test data ground truth, as shown in Table D1. **Table D2.** highlights the predictive accuracy of the model at the time of diagnostic scan, which varies from patient-to-patient. In this case, the neural network model also achieved the highest predictive accuracy, R^2 of 0.60. Fig. B1 shows an example of a test patient's prediction curve and their clinical data (ground truth). Fig. C1 shows the plots of predicted versus actual contrast enhancement of all the clinical data points (multiple points per patient) of both the top performing neural network model and the PBPK model to evaluate the accuracy of the overall curve on the test dataset. We found the predictive accuracy of the neural network model to be greater than the PBPK model (R^2 = 0.61 and 0.11, respectively). Fig. D1 shows the predicted versus actual contrast enhancements at time of diagnostic scan (only one point per patient). Similarly in this case, the neural network model predictive accuracy was greater than the PBPK model (R^2 = 0.60 and 0.01, respectively). **Table D2.** highlights the prediction accuracy at time of scan for the different algorithm method we used to train the model.

4.2. *Clinical implication*

Among the 1577 patient cases we used for the study, we found that 28 % of the patients from our library were under-enhanced (<92 HU), while 8 % were over-enhanced (>132 HU) during their diagnostic scans. The $CTDI_{vol}$ ranged between 4.11 mGy and 58.6 mGy with a median of 14.7 mGy, while the organ dose-based effective dose ranged between 2.5 mSv and 34.7 mSv with a median value of 8.54 mSv. Using our predictive model to retrospectively and theoretically adjust the concentration of contrast media was shown to reduce the coefficient of variation of the liver enhancement across test set patients by 38 % compared to actual levels of enhancement at time of diagnostic scan, as shown by Fig. E1. Further, the results indicated that an 50 % reduction could be achieved in the number of over-enhancements and about 84 % reduction could be achieved in the number of under enhancement. Using

the Kruskal Wallis test, the resulting test patient population of enhanced consistency were found to be statistically significant ($p < 0.001$) as compared to the original test patient.

5. Discussion

This study built and demonstrated a model of contrast enhancement in CT based on clinical data and pharmacokinetic models of contrast perfusion. Overall, the results indicated that a hybrid data- and principle-informed approach can provide an improvement in modeling the enhancement process without requiring bolus tracking data from test patients. In addition, the method proved to offer a simple heuristic approach requiring less computational resources to train and predict, compared to the relatively complex PBPK differential equations. The study also demonstrated the potential utility of such a model to improve the consistency of contrast enhancement, as demonstrated in Fig. E1. In the clinical practice, having a more complete prediction curve could further complement the usage of the current bolus tracking methods to guide the practitioner in determining the optimal time to conduct the scan and in adjusting the contrast administration as needed. This adjustment could be in the form of using a contrast media with different concentration, changing the injection flow rate and volume of the contrast media, or adjusting the diagnostic scan time. Future extensions of the study will include such prospective testing on patients undergoing contrast-enhanced CT scan.

There are several limitations to this study. First, our dataset only came from one institution. Future studies may include patient data from multiple institutions to ensure a more robust model. Second, while numerous studies have demonstrated the importance of weight to predict contrast dynamics in different patients, there are other factors which we did not include in the study due to unavailability of data, including cardiac function measurements (blood pressure, heart rate), hydration levels, and pre-existing conditions which might affect the perfusion of the contrast media. Third, we did not consider liver abnormalities or diseases in our study. Certain liver diseases, such as hepatic cirrhosis, may influence contrast perfusion both in the liver and other organs, and thus additional training of the model can provide more accurate perfusion model for patient sub-groups. Finally, while using the PBPK model has allowed us to create a prediction curve beyond the time window of our clinical data availability, the clinical accuracy of the prediction curve where we have no clinical data of (e.g., delayed/equilibrium phase) remains unvalidated due to lack of ground truth. Future studies may include more data points for each patient to validate the delayed phases of imaging.

6. Conclusion

Clinical inconsistencies in organ contrast enhancement can potentially expose patients to clinical and safety risks, such as missed diagnosis, contrast-induced toxicity, and unnecessary additional dose from repeated scans for under-enhanced patients [12,23,24]. In this paper, we have demonstrated the possibility of utilizing a mechanistic and data-driven contrast enhancement prediction model using *a priori*-known patient information to improve the consistency of clinical CT examinations.

Ehsan Samei lists relationships with the following entities unrelated to the present publication: GE, Siemens, Imalogix, 12Sigma, SunNuclear, Metis Health Analytics, Cambridge University Press, Wiley and Sons.

Daniele Marin has received a research grant from Siemens Healthineers unrelated to present publication.

This work is funded through the NIH grant R01-EB001838, NIH/NIBIB grant *P*41-EB028744, and funding from Bracco Diagnostics, Monroe Township NJ, USA.

Ethical Adherence:

This study was performed under the approval of Duke University Health System Institutional Review Board (IRB).

Declaration of Competing Interest

The authors declare that they have no known competing financial interests or personal relationships that could have appeared to influence the work reported in this paper.

References

[1] P. Sahbaee, E. Samei, W. Segars, SU-C-12A-03: the impact of contrast medium on radiation dose in CT: a systematic evaluation across 58 patient models, Medical Physics 41 (2014) 106.
[2] Y. Yanaga, K. Awai, Y. Nakayama, T. Nakaura, Y. Tamura, M. Hatemura, Y. Yamashita, Pancreas: patient body weight tailored contrast material injection protocol versus fixed dose protocol at dynamic CT, Radiology 245 (2) (2007) 475–482.
[3] Y. Yamashita, Y. Komohara, M. Takahashi, M. Uchida, N. Hayabuchi, T. Shimizu, I. Narabayashi, Abdominal helical CT: evaluation of optimal doses of intravenous contrast material–a prospective randomized study, Radiology 216 (3) (2000) 718–723.
[4] T. Ichikawa, S.M. Erturk, T. Araki, Multiphasic contrast-enhanced multidetector-row CT of liver: contrast-enhancement theory and practical scan protocol with a combination of fixed injection duration and patients' body-weight-tailored dose of contrast material, Eur J Radiol 58 (2) (2006) 165–176.
[5] E. Arana, L. Martí-Bonmatí, E. Tobarra, C. Sierra, Cost reduction in abdominal CT by weight-adjusted dose, Eur J Radiol 70 (3) (2009) 507–511.
[6] L.M. Ho, R.C. Nelson, D.M. Delong, Determining contrast medium dose and rate on basis of lean body weight: does this strategy improve patient-to-patient uniformity of hepatic enhancement during multi-detector row CT? Radiology 243 (2) (2007) 431–437.
[7] S.K. Tan, K.H. Ng, C.H. Yeong, R.R.A. Raja Aman, F. Mohamed Sani, Y.F. Abdul Aziz, Z. Sun, Personalized administration of contrast medium with high delivery rate in low tube voltage coronary computed tomography angiography, Quant Imaging Med Surg 9 (4) (2019) 552–564.
[8] H. Kondo, M. Kanematsu, S. Goshima, Y. Tomita, M.-J. Kim, N. Moriyama, M. Onozuka, Y. Shiratori, K.T. Bae, Body size indexes for optimizing iodine dose for aortic and hepatic enhancement at multidetector CT: comparison of total body weight, lean body weight, and blood volume, Radiology 254 (1) (2010) 163–169.
[9] J.F. Platt, K.A. Reige, J.H. Ellis, Aortic enhancement during abdominal CT angiography: correlation with test injections, flow rates, and patient demographics, AJR Am J Roentgenol 172 (1) (1999) 53–56.
[10] M. Kormano, K. Partanen, S. Soimakallio, T. Kivimäki, Dynamic contrast enhancement of the upper abdomen: effect of contrast medium and body weight, Invest Radiol 18 (4) (1983) 364–366.
[11] K.T. Bae, Optimization of contrast enhancement in thoracic MDCT, Radiol Clin North Am 48 (1) (2010) 9–29.
[12] R. Kessler, et al., Patient body weight-tailored contrast medium injection protocol for the craniocervical vessels: a prospective computed tomography study, PLoS One 9 (2) (2014) e88867.
[13] L. Laurent, et al., Weight-based contrast administration in the computerized tomography evaluation of acute pulmonary embolism: Challenges in optimizing imaging quality, Medicine (Baltimore) 96 (5) (2017) e5972.
[14] P. Sahbaee, W.P. Segars, E. Samei, Patient-based estimation of organ dose for a population of 58 adult patients across 13 protocol categories, Med Phys 41 (7) (2014), 072104.
[15] K.T. Bae, J.P. Heiken, J.A. Brink, Aortic and hepatic contrast medium enhancement at CT. Part I. prediction with a computer model, Radiology 207 (3) (1998) 647–655.
[16] Sahbaee, P., et al., *The Effect of Contrast Material on Radiation Dose at CT: Part I. Incorporation of Contrast Material Dynamics in Anthropomorphic Phantoms.* Radiology, 2017. **283**(3): p. 739-748.
[17] Setiawan, H., et al., *Patient-informed and physiology-based modelling of contrast dynamics in cross-sectional imaging.* SPIE Medical Imaging. Vol. 10948. 2019: SPIE.
[18] H. Setiawan, et al., Modeling patient-informed liver contrast perfusion in contrast-enhanced computed tomography, J Computer Assisted Tomography 44 (6) (2020) 882–886.
[19] *The 2007 Recommendations of the International Commission on Radiological Protection, ICRP Publication 103*. 2007: Ann. ICRP. p. 9-34.
[20] Fu, W., et al. *From patient-informed to patient-specific organ dose estimation in clinical computed tomography*. in *Society of Photo-Optical Instrumentation Engineers (SPIE) Conference Series*. 2018.
[21] K.T. Bae, Intravenous contrast medium administration and scan timing at CT: considerations and approaches, Radiology 256 (1) (2010).
[22] Y. Cheng, et al., Validation of algorithmic CT image quality metrics with preferences of radiologists, Med Phys 46 (11) (2019) 4837–4846.
[23] S.T. Feng, et al., An Individually Optimized Protocol of Contrast Medium Injection in Enhanced CT Scan for Liver Imaging, Contrast Media Mol Imaging (2017) 7350429.
[24] R. Solomon, G. Deray, How to prevent contrast-induced nephropathy and manage risk patients: practical recommendations, Kidney Int Suppl 100 (2006) S51–S53.